Journal of Aeronautics and Space Technologies

15(2) (2022) 13-27

Journal Homepage: jast.hho.msu.edu.tr

RESEARCH ARTICLE

Sun-Direction Estimation under the Effect of Lunar Albedo

Ay Albedosu Etkisinde Güneş'e Yönelme Vektörü Kestirimi

Demet Çilden Güler[1*]

[1] *Istanbul Technical University, Department of Astronautical Engineering, 34469 Istanbul, Turkey*

Received: *March 24, 2022* ***Revised:*** *May 10, 2022* ***Accepted:*** *May 27, 2022*

Abstract

Spacecraft or the instruments are directed to certain directions or points in order to successfully complete their mission. Solar sensors are commonly used as they are capable of being used in planetary or interplanetary space missions in the solar system. Mostly, these instruments sense not only the radiation from the sun but also the albedo of any nearby object. These measurements are known to cause erroneous outputs in the attitude and control system when used without considering the albedo model. In this study, the effect of the lunar albedo on the sun sensor and sun direction estimation is evaluated under different simulation conditions.

Keywords: Spacecraft, Moon, Albedo, Attitude Determination, Sun-Direction Estimation, EKF, UKF

Özet

Uzay araçları veya üzerindeki aletler görevlerini başarılı bir şekilde sürdürmek ve tamamlamak için belirli yönlere veya noktalara yönlendirilmektedirler. Güneş sensörleri, güneş sistemindeki hem gezegen etrafında seyreden uydularda hem de gezegenler arası uzay görevlerinde kullanılabildiğinden tercih edilmektedirler. Bunlardan birçoğu yalnızca güneşten gelen radyasyonu değil yakınındaki herhangi bir objenin albedosunu da ölçmektedir. Bu ölçümlerin, yönelim belirleme ve kontrol bilgisayarında, albedo modelinin dikkate alınmadan kullanılması durumunda hataya sebep olduğu bilinmektedir. Bu çalışmada, Ay albedosunun güneş sensörü ve güneşe yönelme vektörü kestirimi üzerindeki etkisi farklı benzetimler üzerinden değerlendirilmiştir.

Anahtar Kelimeler: Uzay Aracı, Ay, Albedo, Yönelim Belirleme, Güneş'e Yönelme Vektörü Kestirimi, EKF, UKF

1. INTRODUCTION

The interest in cislunar space, Moon's orbit and landing is increasing due to many reasons such as interplanetary mission staging, exploration of Moon, Earth-Moon gateway [1–3]. A planetary CubeSat mission is being developed to reach Moon by National Aeronautics and Space Administration (NASA) Jet Propulsion Laboratory, called Lunar Flashlight [4]. The guidance navigation and control (GNC) system is presented in [5]. The CubeSat with four-channel laser projector will be designed to illuminate permanently shadowed Moon regions for measuring surface reflectance at wavelengths where water ice absorbs.

A GNC system is presented in [6] for six degrees of freedom rendezvous in multi-body cislunar space. Relative navigation methods based on only vision are applied, in that study, using a simple suite of sensors for a coupled state estimation. An attitude

*Corresponding Author
E-mail: dmtcldn@gmail.com

estimation algorithm and the attitude calibration maneuvers are developed in [7] for NASA's Orion mission with an observability analysis while processing star tracker measurements. The analysis of the study shows that the states are observable and can be estimated when the gyroscope biases and scale factors drift at different rates in addition to first-order Gauss–Markov process modeling of the inertial measurement unit to star tracker misalignments. Coarse alignment methods for lunar rovers are examined in [8] based on sun sensors and accelerometers. In most of the alignment processes, the acceleration and rotation rate of the stationary rover is used as reference vectors, which is found to be less accurate for the Moon because of its small rotation rate with respect to Earth.

The sunlight is commonly assumed as the only light source for the satellite observations around Earth even though the reflected light from Earth and Moon would increase the errors in the estimations of the satellite's state. Therefore, the impact of the earthshine and moonlight under varying attributes of satellites is investigated in [9]. Earthshine at the Moon is an illumination source for optical measurements in shadowed lunar areas [10]. The effects of a planet's albedo are investigated in several studies for different purposes using different tools [11–18]. In [12], sun sensor and magnetometer are used for three axes attitude determination. The sun sensor consists of six solar cells placed on each surface of the satellite. As the largest error source, Earth's albedo is numerically modeled based on the reflectivity coefficient, the satellite's position, and the sun's position as a polynomial function. An albedo model is also presented by [13] with validation from Orsted satellite telemetry. An attitude estimation method based on an unscented Kalman filter (UKF), using gyroscope, magnetometer, and solar panels as sun sensors considering the Earth's albedo is presented in [14]. However, that work does not consider the case of eclipses. Another attitude estimation method is proposed in [15] that also estimates the albedo in two stages without any albedo coefficient data, spacecraft position, sky condition, or ground coverage. A neural network-based method is presented in [16] for sun sensor measurement correction. A method is presented in [17] for determining the albedo on the sun sensor measurements using another attitude sensor, magnetometer. Reviewing these studies show that this topic still needs further investigation, especially for the celestial bodies other than Earth. In this study, a Moon-orbiting satellite is, therefore, considered for analyzing the albedo effects on the sun sensor outputs and the estimation of the sun direction.

The structure of this paper is organized as follows. Section 2 presents the mathematical models of spacecraft dynamics and sun sensor measurement model respectively. Section 3 introduces the Gaussian estimation filter formulations. In Section 4, the analysis and results of several scenarios for the albedo effects on sun sensors, and estimation filters are presented and discussed. Section 5 concludes the paper with a summary of the important outputs and future work.

2. MATHEMATICAL MODELS FOR THE SATELLITE'S ROTATIONAL MOTION

2.1. Equations of Rotational Motion

The kinematic equations are derived using Modified Rodrigues parameters (MRPs) [19, 20]. First, we can define the MRP vector $(\mathbf{p})$ in terms of quaternions $(\mathbf{q})$,

$$p_i = \frac{q_i}{1+q_0} \qquad i = 1,2,3 \tag{1}$$

The kinematic differential equations in terms of MRPs with the explicit matrix formulation can be expressed as,

$$\dot{\mathbf{p}} = \frac{1}{4}\begin{bmatrix} \left(1+p_1^2-p_2^2-p_3^2\right) & 2\left(p_1p_2-p_3\right) & 2\left(p_1p_3+p_2\right) \\ 2\left(p_2p_1+p_3\right) & \left(1-p_1^2+p_2^2-p_3^2\right) & 2\left(p_2p_3-p_1\right) \\ 2\left(p_3p_1-p_2\right) & 2\left(p_3p_2+p_1\right) & \left(1-p_1^2-p_2^2+p_3^2\right) \end{bmatrix}\begin{bmatrix} \tilde{\omega}_1 \\ \tilde{\omega}_2 \\ \tilde{\omega}_3 \end{bmatrix} \tag{2}$$

where $\boldsymbol{\omega}_{BR} = \begin{bmatrix} \tilde{\omega}_1 & \tilde{\omega}_2 & \tilde{\omega}_3 \end{bmatrix}^T$ represents the body angular velocity components with respect to the reference frame. The transformation can be performed using the relationship between $\boldsymbol{\omega}_{BI} = \begin{bmatrix} \omega_1 & \omega_2 & \omega_3 \end{bmatrix}^T$ and $\boldsymbol{\omega}_{BR}$,

$$\boldsymbol{\omega}_{BR} = \boldsymbol{\omega}_{BI} - \mathbf{C}\begin{bmatrix} 0 \\ -\omega_o \\ 0 \end{bmatrix} \tag{3}$$

where $\mathbf{C}$ is the transformation matrix from reference to body coordinates, ω_o is the orbital angular velocity calculated as $\omega_o = \left(\mu / r_0^3\right)^{1/2}$ having μ as the product of the universal gravitational constant and the mass of Moon, and r_0 as the distance between the satellite and Moon's center of mass. The dynamic relations can be obtained by the principle of the conservation of angular momentum. By adding the acting external torques,

$$J_1 \frac{d\omega_1}{dt} = N_1 + \left(J_2 - J_3\right)\omega_2\omega_3, \tag{4}$$

$$J_2 \frac{d\omega_2}{dt} = N_2 + \left(J_3 - J_1\right)\omega_3\omega_1, \tag{5}$$

$$J_3 \frac{d\omega_3}{dt} = N_3 + \left(J_1 - J_2\right)\omega_1\omega_2 \tag{6}$$

where J_1, J_2 and J_3 are the terms of the principal moment of inertia, N_1, N_2 and N_3 are the terms of the external disturbances affecting the satellite. In this study, only the body gravity of Moon is taken into consideration [21] with around 1/6 magnitude of Earth's.

2.2. Sun Sensor Measurement Model

Coarse sun sensors have output currents that are proportional to the angle between the sensor's boresight and the direction of the light source [22]. The solar irradiance formulation on the sun sensor position is $F_{\text{sun}}\left(\hat{\mathbf{s}}_{SS}\cdot\hat{\mathbf{n}}_{SS}\right)$ where F_{sun} is the solar constant where the lunar-surface solar irradiance ranges from 1308.9 W/m^2 to 1425.7 W/m^2 [23], $\hat{\mathbf{s}}_{SS}$ is the sun direction vector from the sun sensor, $\hat{\mathbf{n}}_{SS}$ is the unit normal vector of the sun sensor. The generated current of the sun sensor is then,

$$I_d=\begin{cases} I_{\max}\dfrac{F_{\text{sun}}}{F_{\text{cal}}}\left(\hat{\mathbf{s}}_{\text{SS}}\cdot\hat{\mathbf{n}}_{\text{SS}}\right) & \text{if } \left(\hat{\mathbf{s}}_{\text{P}}\cdot\hat{\mathbf{n}}_{\text{A}}>0\right)\cap\left(\hat{\mathbf{s}}_{\text{SS}}\cdot\hat{\mathbf{n}}_{SS}\geq\cos(\Delta)\right) \\ 0 & \text{otherwise} \end{cases} \tag{7}$$

where F_{cal} is the calibration flux determined in ground testing, $I_{\max}$ is the maximum output current of the sun sensor, $\hat{\mathbf{s}}_{\text{P}}$ is the sun direction vector from the celestial object, $\hat{\mathbf{n}}_{\text{A}}$ is the unit normal vector of the differential area on the celestial object, Δ is the half-field of view angle. The current of the sun sensor because of the albedo is [13],

$$I_\alpha=\begin{cases} I_{\max}\dfrac{F_{\text{sun}}}{F_{\text{cal}}}\displaystyle\sum_{i=1}^{N_A}\frac{\alpha\left(\hat{\mathbf{s}}_{\text{P}}\cdot\hat{\mathbf{n}}_{\text{A}_i}\right)\left(\hat{\mathbf{r}}_{\text{AS}_i}\cdot\hat{\mathbf{n}}_{\text{A}_i}\right)\left(-\hat{\mathbf{r}}_{\text{AS}_i}\cdot\hat{\mathbf{n}}_{SS}\right)}{\pi\left\|\mathbf{r}_{\text{AS}_i}\right\|^2}\Delta A, & \text{if } \Delta A\in A \\ 0 & \text{if } \Delta A\notin A \end{cases} \tag{8}$$

where $\mathbf{r}_{\text{AS}}$ is the sun sensor's position vector from the differential area on the celestial body with the unit direction vector of $\hat{\mathbf{r}}_{\text{AS}}=\dfrac{\mathbf{r}_{\text{AS}}}{\left\|\mathbf{r}_{\text{AS}}\right\|}$, α is the albedo coefficient of the celestial body. For the albedo coefficients for Moon, the Lunar Orbiter Laser Altimeter (LOLA) on Lunar Reconnaissance Orbiter (LRO) can be used that is principally a laser altimeter but also measures the strength of the returned laser pulse reflected by the Moon at 1064 nm wavelength [24–26]. The permanent shadow areas in the polar regions of the Moon are found to be more reflective than the polar surfaces that are sometimes illuminated [25].

By adding the albedo contribution on the sun sensor, the current of each sensor can be calculated as,

$$I=I_d+I_\alpha+\varepsilon_{CSS}, \tag{9}$$

where ε_{CSS} is zero-mean Gaussian noise on the measurements.

For more than one sun sensor and especially when using a sun sensor platform, the sun direction measurements can be summed up to the vector as,

$$\mathbf{y}_{SS}=\sum_{i=1}^{N_{\text{SS}}}I_i\cdot\hat{\mathbf{n}}_{\text{SS}_i}, \tag{10}$$

where N_{SS} is the number of sun sensors.

3. FORMULATION OF THE ESTIMATION FILTER

The estimation problem in general state-space form is expressed as,

$$\mathbf{x}_k = f\left(\mathbf{x}_{k-1}\right) + \mathbf{w}_k, \tag{11}$$

$$\mathbf{y}_k = h_k\left(\mathbf{x}_k\right) + \boldsymbol{\varepsilon}_k, \tag{12}$$

where $f(\cdot)$ is the process and $h(\cdot)$ is the measurement function, $\mathbf{x}_k$ is the state vector at a time t_k, $\mathbf{w}_k$ is the zero-mean Gaussian noise vector with the covariance of $\mathbf{Q}$, $\mathbf{y}_k$ is the measurement vector, and $\boldsymbol{\varepsilon}_k$ is the zero-mean Gaussian noise vector with the covariance of $\mathbf{R}_k$. The state vector to be estimated is chosen to be the sun direction vector on the sun sensor frame as,

$$\mathbf{x}_k = \left[\hat{\mathbf{s}}_{SS_k}\right] \tag{13}$$

The initial state is $\mathbf{x}_0$ with mean $\boldsymbol{\mu}_0$ and covariance $\mathbf{P}_0$. The predictions using the process function can be found as,

$$\boldsymbol{\mu}_k^- = \int f\left(\mathbf{x}_{k-1}\right) \mathrm{N}\left(\mathbf{x}_{k-1} \middle| \boldsymbol{\mu}_{k-1}, \mathbf{P}_{k-1}\right) d\mathbf{x}_{k-1}, \tag{14}$$

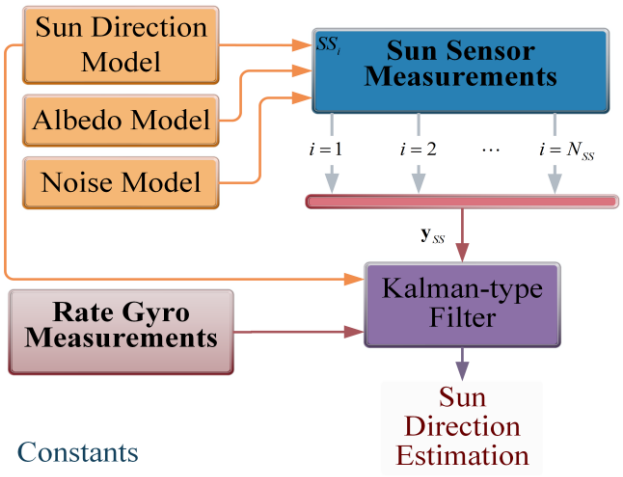


Figure 1. The block diagram of the sun direction estimation using a Kalman-type filter.

with the predicted covariance,

$$\mathbf{P}_k^- = \int \left(f\left(\mathbf{x}_{k-1}\right) - \boldsymbol{\mu}_{k-1}\right)\left(f\left(\mathbf{x}_{k-1}\right) - \boldsymbol{\mu}_{k-1}\right)^T \mathrm{N}\left(\mathbf{x}_{k-1} \middle| \boldsymbol{\mu}_{k-1}, \mathbf{P}_{k-1}\right) d\mathbf{x}_{k-1} + \mathbf{Q}. \tag{15}$$

The predictions are then updated using the measurements as,

$$\hat{\mathbf{y}}_k = \int \mathbf{h}_k\left(\mathbf{x}_k\right) \mathrm{N}\left(\mathbf{x}_k \middle| \boldsymbol{\mu}_k^-, \mathbf{P}_k^-\right) d\mathbf{x}_k, \tag{16}$$

$$\boldsymbol{\Psi}_k = \int \left(\mathbf{x}_k - \boldsymbol{\mu}_k^-\right)\left(\mathbf{h}_k\left(\mathbf{x}_k\right) - \hat{\mathbf{y}}_k\right)^T \mathrm{N}\left(\mathbf{x}_k \middle| \boldsymbol{\mu}_k^-, \mathbf{P}_k^-\right) d\mathbf{x}_k, \tag{17}$$

$$\mathbf{\Phi}_k = \int \left(\mathbf{h}_k\left(\mathbf{x}_k\right) - \hat{\mathbf{y}}_k\right)\left(\mathbf{h}_k\left(\mathbf{x}_k\right) - \hat{\mathbf{y}}_k\right)^T \mathrm{N}\left(\mathbf{x}_k \middle| \boldsymbol{\mu}_k^-, \mathbf{P}_k^-\right) d\mathbf{x}_k. \tag{18}$$

The innovation is,

$$\mathbf{e}_k = \mathbf{y}_k - \hat{\mathbf{y}}_k, \tag{19}$$

with the covariance,

$$\mathbf{S}_k = \mathbf{\Phi}_k + \mathbf{R}_k. \tag{20}$$

Then, the Kalman gain can be determined as,

$$\mathbf{K}_k = \mathbf{\Psi}_k \mathbf{S}_k^{-1}. \tag{21}$$

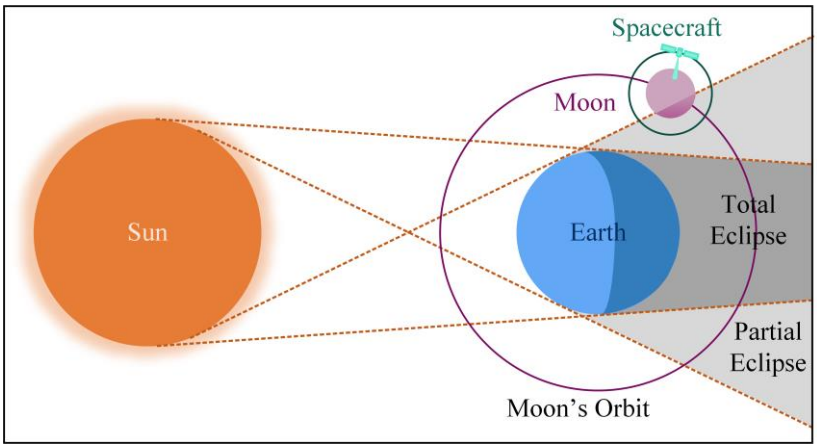


Figure 2. Exemplary representation of the eclipse areas caused by Earth when Earth shadows the Moon's orbit, and spacecraft's orbit around Moon.

The posterior mean and the associated covariance are,

$$\boldsymbol{\mu}_k = \boldsymbol{\mu}_k^- + \mathbf{K}_k \mathbf{e}_k, \tag{22}$$

$$\mathbf{P}_k = \mathbf{P}_k^- - \mathbf{K}_k \mathbf{S}_k \mathbf{K}_k^T, \tag{23}$$

The integrals in Eqs. (14) to (18) can be approximated using Kalman filters [27–29]. The direction of the sun can be estimated using conventional approaches, e.g. extended Kalman filter (EKF) and UKF using nonlinear process and measurement functions. Both EKF and UKF are used in this study using the flow presented in Figure 1. As seen from the figure, the sun sensor measurements are modeled based on the sun direction model, albedo model and the noise model that are than processed under a Kalman-type filter with the rate gyro measurements for estimating the sun direction. The constant values used in all the processes are indicated on the bottom left of the figure.

4. ANALYSIS AND RESULTS

A spacecraft reached to lunar orbit is simulated for an examination of the Moon's albedo effects on its sun sensor outputs. In this study, we considered a hypothetical spacecraft with the mass moment of inertia $J = \text{diag}\left(\begin{bmatrix}900 & 800 & 600\end{bmatrix}\right)$ kg.m^2 beginning the orbit at July 13, 2021 "00:00:0.0 UTC". The simulation is initialized with the state vector of $\mathbf{x}_0^{\text{true}} = \begin{bmatrix}0 & 0 & 0 & 0 \text{ deg/}s & 0 \text{ deg/}s & 0.5 \text{ deg/}s\end{bmatrix}^T$. In this study, hypothetical coarse sun sensors are modeled based on the introduced measurement model. As the available lunar albedo data is at 1064 nm wavelength, the sun sensors are also assumed to be sensitive at 1064 nm. However, the albedo characteristics might be different for various wavelengths e.g. visible light for common usage. There is a potential to have more datasets in near future as Moon missions are paid attention lately. In modeling the sun sensor measurements, it is possible not to take the eclipse case into account. However, for albedo contribution, only the coefficients for the partial eclipse of each grid on the Moon can be eliminated in the calculations. The representation of the partial eclipse on Earth and the orbit of the spacecraft around Moon is shown in Figure 2. This is merely a sketch to demonstrate a broad perspective of total and partial eclipse scenarios when Earth shadows the node on the Moon's orbit; however, the Earth's eclipse effects are not included in the simulation examples. The ephemeris information of the celestial bodies is obtained from the NASA Navigation and Ancillary Information Facility (NAIF) SPICE toolkit [30].

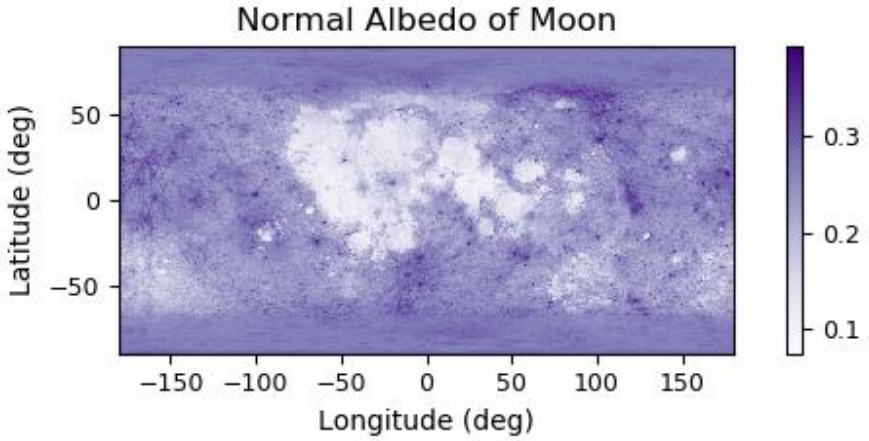


Figure 3. Global normal albedo distribution of Moon (LOLA).

An astrodynamics software, called Basilisk, which is open source and available to everyone, developed in the University of Colorado Boulder, USA with a spacecraft-based fast simulation working framework [31, 32] is used in this study. The software is an astrodynamics architecture that includes fast, repeatable Monte-Carlo simulation options [33]. This software can provide the speed of implementation of the C/C++ language while containing the easy writing and reconfiguration of Python. The albedo module is written in C++ and run with Python user inputs using the SWIG (Simplified Wrapper and Interface Generator) interface. Basilisk is used for,

i. Writing the albedo module in an open source software that is shared with public,

ii. Simulating the spacecraft and necessary models in a fast environment (Python),
iii. Using a holistic software that can link other modules,
iv. Running the whole algorithm.

The derived normal albedo data from LOLA is used as the reflectance measure of the lunar surface. Therefore, the data also includes the regions lacking direct solar illumination. The global albedo distribution is illustrated in Figure 3. The albedo data obtained from LOLA instrument is given as input to the Basilisk software. The analysis is carried out for varying altitudes from 50 km up to 5,000 km in order to determine the critical altitude for the effective albedo acting on the sensors. Here, it should be noted that two albedo packages are used. One is the normal albedo data and the second package is the average albedo coefficient (0.12).

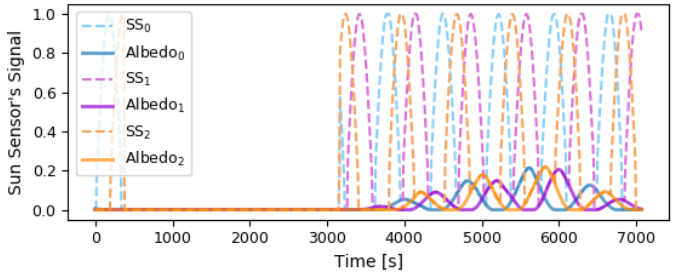


Figure 4. Three sun sensor readings with corresponding albedo interference (Normal albedo data – 100 km altitude).

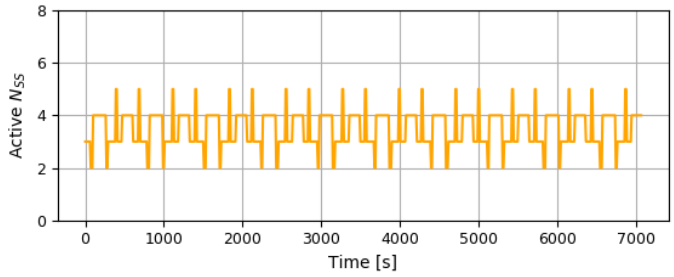


Figure 5. Number of active sun sensors for the orbital period.

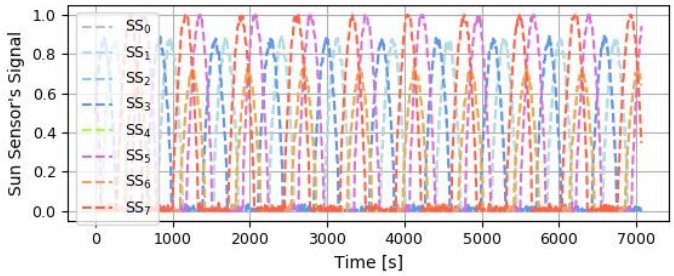


Figure 6. Sun sensor's signal for the nominal case (no albedo).

The spacecraft simulation runs at 100 km altitude to demonstrate one full low Moon orbit. Three sun sensor measurements with their albedo readings can be seen in Figure 4. Here, the normal albedo data is used for the simulations. The maximum albedo readings of the sun sensor are presented in Table 1 for different altitudes to see the critical altitude where the albedo can be negligible. From this table, it can be stated that the albedo is read less than 10% for the altitudes greater than ~500 km.

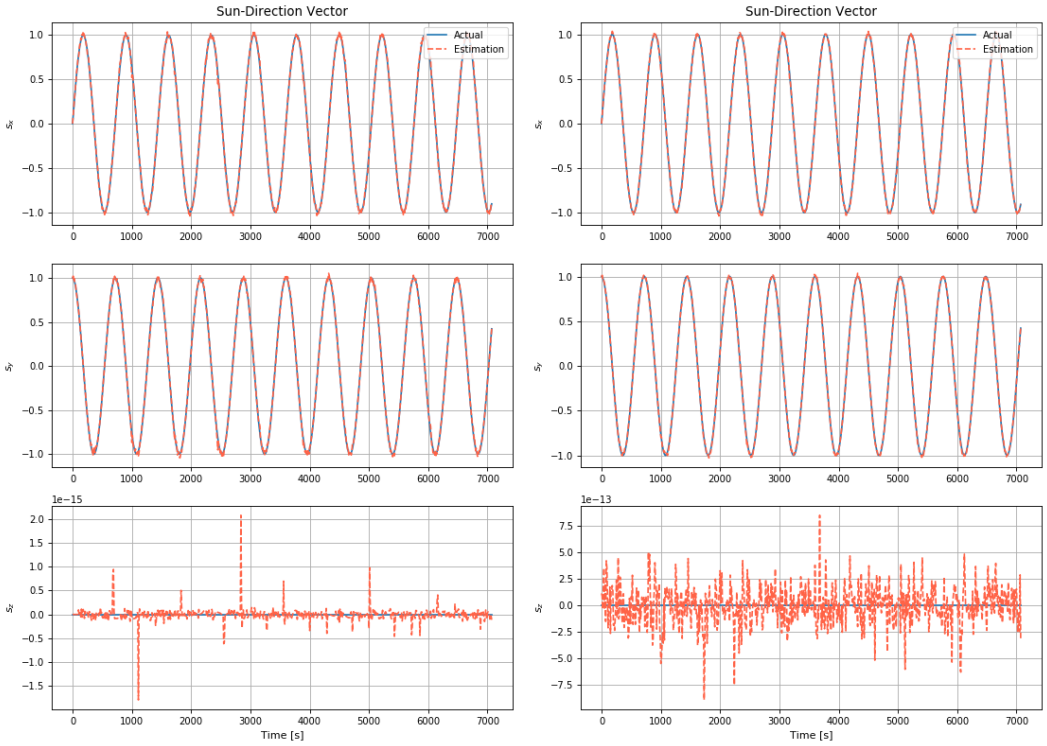


Figure 7. Estimated sun-direction estimation components by EKF (left) and UKF (right) under nominal case.

Table 1. Maximum albedo readings of the sun sensor at different altitudes.

Altitude (km)	i^{th} Sun Sensor Albedo Readings (Maximum)		
	i=0	i=1	i=2
50	0.25	0.21	0.19
100	0.21	0.20	0.21
500	0.13	0.13	0.12
1,000	0.08	0.08	0.08
5,000	0.01	0.01	0.01

Sun-direction estimations are examined for the spacecraft at 100 km altitude in two sections as the nominal case and the lunar albedo case.

4.1. Sun Direction Estimation under Nominal Case

The number of activated sun sensors that receive light and generate signals is presented in Figure 5 for the nominal case without any lunar albedo effects on the sensors. The active

sun sensors are varying between 2-5 out of eight during the entire orbital period. One of the common photodiode configurations is to use orthogonal six sensors for full coverage [34]. However, more than six photodiodes are possibly used on the small satellites. For example, nine sun sensors are used on the 3-unit CubeSat, RAX [35].

Eight sun sensors are implemented for generating signals. The signal intensity is presented in Figure 6. EKF and UKF estimations with corresponding actual values that use these signals are shown in Figure 7. Both estimations have a difference under 0.5 degrees from the actual sun-direction vector.

4.2. Sun Direction Estimation under Lunar Albedo Case

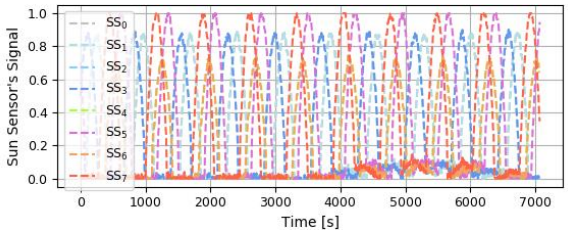


Figure 8. Sun sensor's signal for the average constant albedo case.

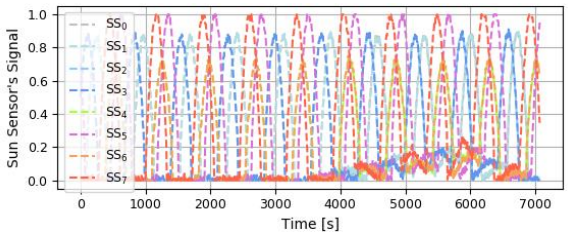


Figure 9. Sun sensor's signal for the normal albedo data case.

The second test is carried out in the presence of lunar albedo. First, the average constant albedo as 12% is used for the simulations. Second, the normal albedo data from LOLA is utilized. The sun sensor's signals for both cases are illustrated in Figures 8 and 9 respectively. As can be seen from these figures, the albedo starts increasing after the 4000th second when we compare them with the nominal case of having no albedo on the measurements. It is also more effective for the albedo data case.

Figure 10 presents the sun-direction estimations by EKF and UKF under the average albedo case. The estimation errors with respect to the nominal case seem clear, especially between 4500 and 6000 seconds where the albedo effects are acting on the sun sensors' signals. The albedo when using the albedo data package is more intense for the signals of the sun sensors; therefore, the estimations are expected to be more erroneous for this case (Figure 11) in the same time interval.

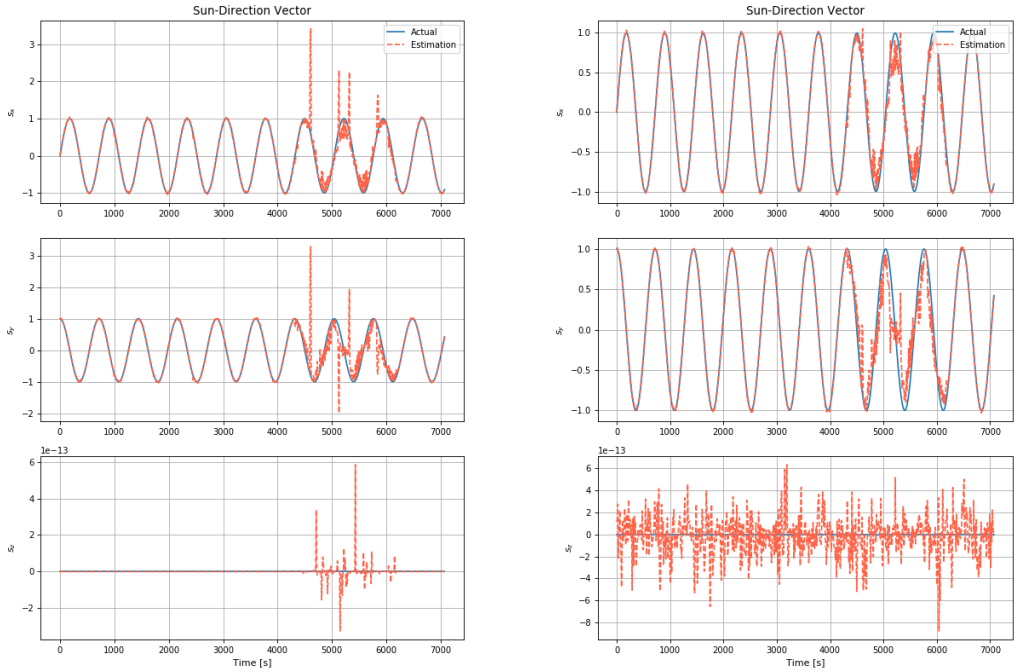


Figure 10. Estimated sun-direction estimation components by EKF (left) and UKF (right) under average albedo case.

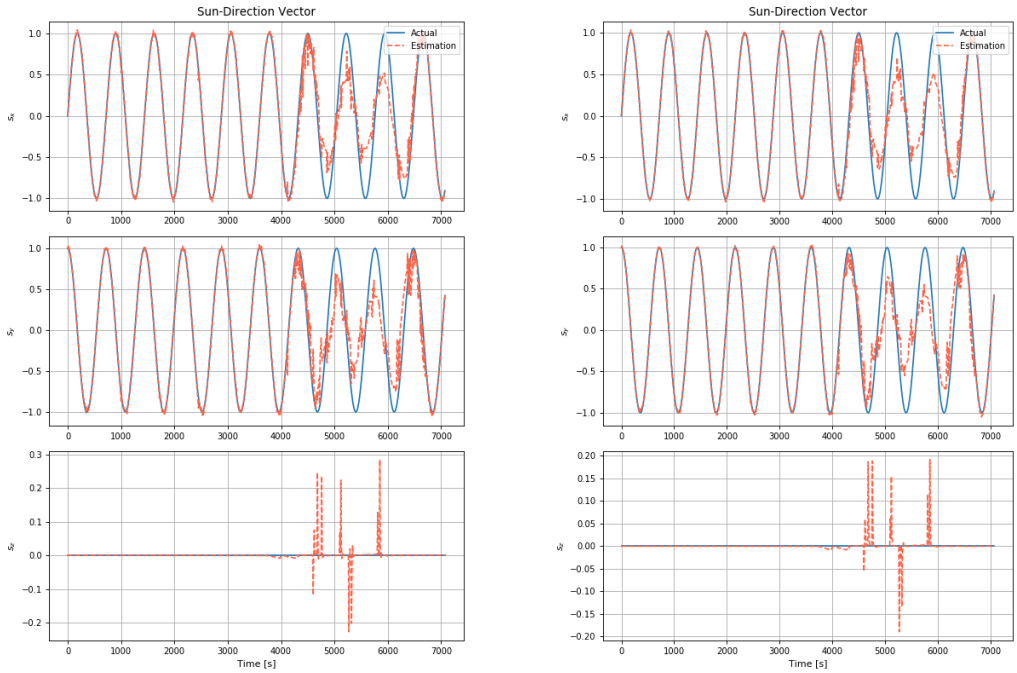


Figure 11. Estimated sun-direction estimation components by EKF (left) and UKF (right) under normal albedo data case.

Table 2. Sun-direction vector estimation errors.

Albedo Package	Error (deg)	
	EKF	UKF
No Albedo	0.309	0.232
Average Constant Albedo	2.125	1.752
Normal Albedo Data	3.143	2.966

Table 2 is composed as a summary of the estimations from EKF and UKF under the albedo-free nominal case and two additional albedo packages. The error is calculated as the average angle difference between the estimated and actual sun-direction vectors. From this table, UKF estimates the sun direction better than EKF but albedo affects the direction estimation results around 3 degrees, which is around 13 times higher than the nominal case and almost double of the average albedo case.

5. CONCLUSION

Coarse sun sensors that are mostly used on small spacecraft sense the radiation from the sun and the reflected light from a close object such as a celestial body. At this point, it is significant to consider the albedo model of the close celestial body that the satellite orbiting around. In this research, the lunar albedo effects are investigated in terms of the sun sensor and sun direction estimation by EKF and UKF. The demonstrations show that UKF estimates the sun-direction vector more accurately than EKF but might still give a 3-degree estimation error under the albedo influence. This means that the lunar albedo especially at low altitudes still needs to be taken into account for sun-direction estimations, whereas the effects get smaller at higher altitudes (~500 km) and might be negligible. In future work, more demonstrations on the varying altitudes and orbits can be investigated further. Another interesting study would be to examine different eclipse cases for the spacecraft with Earth-Moon interactions.

REFERENCES

[1] J. C. Crusan et al., "Deep space gateway concept: Extending human presence into cislunar space" in *Proceedings, IEEE Aerospace Conference*, *IEEE, Big Sky, MT, USA*, *March 3-10, 2018*. pp. 1–10.

[2] H. M. Brown et al., *Resource potential of lunar permanently shadowed regions*, Icarus **377**, 114874 (2022).

[3] A. Rubinsztejn and R. Sood, "Chaining Moon-to-Moon Trajectories Using Network Analysis", in *AIAA SciTech Forum and Exposition, San Diego, CA, January 2-7, 2022*.

[4] "Lunar Flashlight Mission Information." [Online]. Available: https://www.jpl.nasa.gov/missions/lunar-flashlight. [Accessed: March 6, 2022].

[5] P. C. Lai, D. C. Sternberg, R. J. Haw, E. D. Gustafson, P. C. Adell, and J. D. Baker, *Lunar Flashlight CubeSat GNC system development*, Acta Astronautica **173**, 425–441 (2020).

[6] A. Colagrossi, V. Pesce, L. Bucci, F. Colombi, and M. Lavagna, *Guidance, navigation and control for 6DOF rendezvous in Cislunar multi-body environment*, Aerospace Science and Technology **114**, 106751 (2021).

[7] R. Zanetti and C. N. D'Souza, *Observability Analysis and Filter Design for the Orion Earth-Moon Attitude Filter*, Journal of Guidance, Control, and Dynamics, **39**(2), 201–213 (2016).
[8] J. Cha, S. Heo, and C. G. Park, "Coarse alignment of lunar exploration rover using accelerometer and sun sensor", in *International Conference on Control, Automation and Systems, eju, Korea (South), IEEE October 18-21, 2017.* pp. 465–470.
[9] X. Wang, C. Xu, Y. Huo, Y. Wan, Y. Liu, and J. Fu, *Influence of Indirect Solar Irradiance on Satellite Observation*, IEEE Access **9**, 163893–163905 (2021).
[10] D. A. Glenar, T. J. Stubbs, E. W. Schwieterman, T. D. Robinson, and T. A. Livengood, *Earthshine as an illumination source at the Moon*, Icarus **321**, 841–856 (2019).
[11] H. L. Fisher, K. L. Musser, and M. D. Shuster, *Coarse attitude determination from earth albedo measurements*, IEEE Transactions on Aerospace and Electronic Systems **29**(1), 22–26 (1993).
[12] P. Appel, *Attitude estimation from magnetometer and earth-albedo-corrected coarse sun sensor measurements*, Acta Astronautica **56**(1–2), 115–126 (2005).
[13] D. Bhanderi, "Modeling Earth Albedo Currents On Sun Sensors for Improved Vector Observation," in *AIAA Guidance, Navigation, and Control Conference and Exhibit, Keystone, Colorado, August 21-24, 2006.*
[14] L. Baroni, *Attitude determination by unscented Kalman filter and solar panels as sun sensor*, The European Physical Journal Special Topics **229**(8), 1501–1506 (2020).
[15] D. Cilden-Guler, H. Schaub, C. Hajiyev, and Z. Kaymaz, *Attitude Estimation with Albedo Interference on Sun Sensor Measurements*, Journal of Spacecraft and Rockets **58**(1), 148–163 (2021).
[16] S. N. Sozen, M. Gokce, C. Yavuzyilmaz, F. Gulmammadov, and H. E. Soken, "Measurement correction of a set of analog sun sensors via neural network", *2021 IEEE 8th International Workshop on Metrology for AeroSpace (MetroAeroSpace), IEEE, Naples, Italy, June 23-25, 2021.* pp. 1-6.
[17] L. Frezza, F. Santoni, and F. Piergentili, *Sun direction determination improvement by albedo input estimation combining photodiodes and magnetometer*, Acta Astronautica **190**, 134–148 (2022).
[18] T. Oikawa, J. BrÃ¶han, G. Dubernet, and K. Yoshida, "Rover orientation estimation using sun sensors for lunar and planetary exploration," in *69th International Astronautical Congress (IAC), Bremen, Germany, October 1-5, 2018.*
[19] H. Schaub and J. L. Junkins, *Stereographic orientation parameters for attitude dynamics: A generalization of the Rodrigues parameters*, The Journal of the Astronautical Sciences **44**(1), 1–19 (1996).
[20] H. Schaub and J. L. Junkins, *Analytical Mechanics of Space Systems*, Second Edition. Reston, VA: American Institute of Aeronautics and Astronautics, 2009.
[21] P. C. Hughes, *Spacecraft Attitude Dynamics*, Mineola, New York: Dover Publications, 2004.
[22] T. W. Flatley and W. A. Moore, "An Earth Albedo Model: A Mathematical Model for the Radiant Energy Input to an Orbiting Spacecraft Due to the Diffuse Reflectance of Solar Radiation From the Earth Below", Technical Memorandum 104596, *National Aeronautics and Space Administration, Goddard Space Flight Center*, Greenbelt, MD,

1994.[Online].Available:https://ntrs.nasa.gov/api/citations/19940020024/downloads/19940020024.pdf [Accessed: March 6, 2022].
[23] X. Li et al., "Condition of Solar Radiation on the Moon" in *Moon, July 2012, Berlin, Heidelberg*, Springer, pp. 347–365.
[24] D. E. Smith et al., *The Lunar Orbiter Laser Altimeter Investigation on the Lunar Reconnaissance Orbiter Mission*, Space Science Review **150**(1), 209–241 (2009).
[25] P. G. Lucey et al., *The global albedo of the Moon at 1064 nm from LOLA*, Journal of Geophysical Research: Planets 119(7), 1665–1679 (2014).
[26] M. Lemelin et al., *Improved calibration of reflectance data from the LRO Lunar Orbiter Laser Altimeter (LOLA) and implications for space weathering*, Icarus, **273**, 315–328 (2016).
[27] E. A. Wan and R. Van Der Merwe, "The unscented Kalman filter for nonlinear estimation," in *Proceedings of the IEEE 2000 Adaptive Systems for Signal Processing, Communications, and Control Symposium (Cat. No.00EX373), IEEE, Lake Louise, AB, Canada, October o4, 2000*. pp. 153–158.
[28] S. J. Julier and J. K. Uhlmann, "New extension of the Kalman filter to nonlinear systems," in *Proceedings of Signal Processing, Sensor Fusion, and Target Recognition VI*, *1997*, pp.3068.
[29] D. Cilden-Guler, M. Raitoharju, R. Piche, and C. Hajiyev, *Nanosatellite attitude estimation using Kalman-type filters with non-Gaussian noise*, Aerospace Science and Technology **92**, 66–76 (2019).
[30] C. H. Acton, *Ancillary data services of NASA's Navigation and Ancillary Information Facility*, Planetary and Space Science **44**(1), 65–70 (1996).
[31] M. C. Margenet, H. Schaub, and S. Piggott, "Modular attitude guidance development using the basilisk software framework," in *AIAA Space and Astronautics Forum and Exposition, Long Beach, California, September 13 – 16, 2016*.
[32] P. W. Kenneally, S. Piggott, and H. Schaub, *Basilisk: A Flexible, Scalable and Modular Astrodynamics Simulation Framework*, Journal of Aerospace Information Systems **17**(9), pp. 496–507 (2020).
[33] Autonomous Vehicle Systems (AVS) Laboratory, "Welcome to Basilisk: an Astrodynamics Simulation Framework — Basilisk 2.1.1 documentation." [Online]. Available: http://hanspeterschaub.info/basilisk/index.html. [Accessed: March 11, 2022].
[34] J. C. Springmann and J. W. Cutler, *Satellite Attitude Determination with Low-Cost Sensors*, University of Michigan, 2013.
[35] J. C. Springmann, A. J. Sloboda, A. T. Klesh, M. W. Bennett, and J. W. Cutler, *The attitude determination system of the RAX satellite*, Acta Astronautica **75**, 120–135 (2012).

To Cite This Article: D. Çilden Güler, *Sun-Direction Estimation under the Effect of Lunar Albedo*, Journal of Aeronautics and Space Technologies **15**(2), 13-27 (2022).

VITAE

Demet Çilden Güler received her BSc and MSc from Istanbul Technical University in 2014 and 2016, respectively. She completed her PhD at Aeronautical and Astronautical Engineering Department, Istanbul Technical University in 2021. She is the author/coauthor of 35 conference and 13 SCI-E journal papers. She was supported by ASELSAN (Military Electronic Industries) and TUBITAK (Scientific and Technological Research Council of Turkey) during her PhD studies. She is one of the 2018 Amelia Earhart Fellows. Her research interest areas are Kalman filtering, attitude determination and control of small satellites, extraterrestrial magnetic field and planets' albedo effects on satellite's attitude, and integrated estimation methods.